Measuring Rod- and Cone-Photoreceptor-Specific Vision in Inherited Retinal Diseases Using a Commercial Perimeter

Vivian Wu,¹ Alejandro J. Roman,¹ Emma L. Galsterer,² Georg Ansari,³ Inbar Erdinest,⁴ Giulia Righetti,² Iryna Viarbitskaya,¹ Robert C. Russell,¹ Rebecca J. Kim,¹ Jacques Charlier,⁵ Kristina Pfau,^{3,6} Krunoslav Stingl,² Eyal Banin,⁴ Maximilian Pfau,^{3,6} Katarina Stingl,² Tomas S. Aleman,¹ and Artur V. Cideciyan¹

Correspondence: Artur V. Cideciyan, Center for Hereditary Retinal Degenerations, Scheie Eye Institute, Department of Ophthalmology, Perelman School of Medicine, University of Pennsylvania, Philadelphia, Pennsylvania 19104, USA:

cideciya@pennmedicine.upenn.edu.

Received: August 7, 2025 Accepted: September 29, 2025 Published: October 17, 2025

Citation: Wu V, Roman AJ, Galsterer EL, et al. Measuring rod- and cone-photoreceptor-specific vision in inherited retinal diseases using a commercial perimeter. *Invest Ophthalmol Vis Sci.* 2025;66(13):31. https://doi.org/10.1167/iovs.66.13.31

Purpose. The primary pathology in most inherited retinal diseases (IRDs) is located within photoreceptors. Standard automatic perimetry (SAP) can measure photoreceptor disease severity but cannot distinguish between rods, long/middle-wavelength (L/M)–sensitive, and short-wavelength (S)–sensitive cones. Herein we developed a protocol that can provide photoreceptor-specific sensitivities.

METHODS. A commercial (unmodified) perimeter was used to develop a clinical protocol that includes five profiles along the vertical meridian, utilizing different chromatic stimuli presented in the dark-adapted state or on adapting backgrounds. Data were recorded by the Perimetry for IRD (PERIRD) consortium in control participants and patients with IRDs.

RESULTS. The protocol was developed by evaluating the relationship between chromatic thresholds and adapting backgrounds using a threshold-versus-intensity paradigm. Five conditions were selected: two-color dark-adapted, red-on-blue, and blue-on-yellow tests in addition to white-on-white SAP. Prediction intervals from control eyes were defined, and physiological ranges over which rod-, L/M-, and S-cone-specific results can be obtained were estimated. Testing in complete achromatopsia, blue-cone monochromacy, and enhanced S-cone syndrome confirmed classic patterns expected from cone diseases. Patients with incomplete achromatopsia showed partially retained L/M- or S-cone function. Patients with retinitis pigmentosa demonstrated use of photoreceptor-specific function to interpret different disease subtypes and stages. Total test time for the protocol was usually under 30 minutes.

Conclusions. Photoreceptor-specific function can be measured over a large dynamic range using a turnkey commercial perimeter and a relatively short, practical protocol that may be introduced into the clinic, translational work, and clinical trials.

Keywords: achromatopsia, perimetry, retinitis pigmentosa, blue cone monochromacy

P hotons arriving from an illuminated scene are focused onto the retina by the cornea and the lens, and then they are absorbed by photoreceptors, which initiate phototransduction cascades, culminating in the activation of interneuronal signaling pathways that reach the brain to provide visual perception. Psychophysical methods in vision are used to relate visual sensations perceived to measured properties of light stimuli. A common psychophysical method is the measurement of the increment threshold, which refers to

an observer's sensitivity to detect a just-noticeable difference in visual stimulation. 1,2

In inherited retinal diseases (IRDs) affecting the outer retina, a reduction in light sensitivity can provide a quantitative measure of photoreceptor dysfunction, as it occurs with disease progression, or an increment in light sensitivity can signal efficacy of an intervention such as gene therapy. Static automated perimetry (SAP)³ stimulates focal regions across the retina, keeps track of the patients' spatial distribution

Copyright 2025 The Authors iovs.arvojournals.org | ISSN: 1552-5783



¹Center for Hereditary Retinal Degenerations, Scheie Eye Institute, Department of Ophthalmology, Perelman School of Medicine, University of Pennsylvania, Philadelphia, Pennsylvania, United States

²University Eye Hospital, Center for Ophthalmology, University of Tübingen, Tübingen, Germany

³Department of Ophthalmology, University of Basel, Basel, Switzerland

⁴Center for Retinal and Macular Degenerations, Department of Ophthalmology, Hadassah Medical Center and Faculty of Medicine, Hebrew University of Jerusalem, Jerusalem, Israel

⁵Metrovision, Perenchies, France

⁶Department of Ophthalmology, University of Bonn, Bonn, Germany

of light sensitivity, and estimates the spatial distribution of retinal disease severity in IRDs. But photoreceptor-specific changes in IRDs are complex, with variably overlapping dysfunction of rods, short (S)– and long/middle-wavelength (L/M)–sensitive cones, ^{4–6} and SAP, with its achromatic stimuli and backgrounds, cannot distinguish between them. The availability of photoreceptor-specific sensitivity measures in the clinic could better define the natural history and spatial distribution of diseases affecting different photoreceptor populations and their potentially different responses to interventions.

To make sensitivity measures more specific, one takes advantage of physiological differences between photoreceptors. Rods are dominant in night vision, whereas cones are dominant in day vision. SAP uses a steady white light adaptation to desensitize the rods, allowing for the measurement of cone-driven function in many eyes. In cone dysfunction syndromes and related conditions, as well as in cone and cone-rod dystrophies, and some forms of Leber congenital amaurosis, however, light sensitivity on a white adapting background may be counterintuitively driven by rods,^{7–10} consistent with experimental studies showing rods signaling over a large range of ambient lights.^{11,12} Of course, research methods using varied chromatic stimuli on a range of chromatic backgrounds can provide cone-specific function, 13,14 but they are time-consuming and require modified or custom-made instruments, making the resulting protocols impractical for use in the clinic. Recently, a turnkey commercial perimeter with built-in chromatic stimuli and chromatic adapting backgrounds became available. Using this perimeter, the current work lays the foundation for measuring and interpreting photoreceptor-specific sensitivity in a practical manner. The streamlined testing protocols and analyses are being developed within an international perimetry

for IRD (PERIRD) consortium of clinics interested in using photoreceptor-specific testing as a tool to better understand these diseases and help the translation of treatments from proof of concept into the clinic.

METHODS

Participants

Healthy participants (n=17, ages 23–59 years; see Supplementary Fig. S1 for details) with no known vision abnormalities and patients with IRDs (n=20, ages 14–66; Table) were included. The study was conducted in accordance with the Declaration of Helsinki and approved by the institutional review boards. Written informed consent was obtained.

Perimeter and Experimental Protocol

Chromatic static perimetry (MonCvONE; Metrovision, Perenchies, France) was used for all experiments. To identify the optimal test setting, preliminary experiments were performed with four narrowband stimuli (440, 500, 600, and 650 nm) under dark-adapted conditions and across a large range of luminances using two backgrounds (455 nm peak blue and 591 nm peak yellow) under a threshold-versusintensity (tvi) paradigm. Stimuli were presented in inferior and superior visual field locations near 12° from fixation. All tvi data were obtained in a single participant, with limited confirmatory tvi data obtained in two additional participants. Based on the preliminary experimental findings, five conditions were selected for clinical testing: WhiteWB, white stimuli on a 10-cd·m⁻² white background; 500DA and 650DA, corresponding to 500- and 650-nm stimuli, respectively, dark-adapted; 440YB, 440-nm stimuli on the 591-nm

TABLE. Characteristics of Patients

ID	Age, Y/Sex	Eye [†]	Diagnosis/ Phenotype	Molecular			BCVA,‡
				Gene	First Allele	Second Allele	logMAR
P1	28/M	OD	cACHM	CNGB3	c.1148delC, p.T383Ifs*13	c.1148delC, p.T383Ifs*13	1.00
P2	38/F	OS	cACHM	CNGA3	c.667C>T, p.R223W	c.848G>T, p.R283L	0.84
P3	66/M	ou	cACHM	CNGA3	c.139C>T, p.Q47*	c.1495C>T, p.R499*	0.80
P4	14/F	OD	iACHM[L/M]	CNGA3	c.1640T>G, p.F547C	c.1669G>A, p.G557R	0.90
P5	42/F	OU	iACHM[L/M]	CNGA3	c.671C>G, p.T224R	c.1106C>G, p.T369S	n/a ^{\$}
P6	19/F	OU	iACHM[S]	CNGA3	c.499delC, p.L167Cfs*6	c.1669G>A, p.G557R	0.80
P 7	34/M	OS	iACHM[S]	CNGA3	c.829C>T, p.R277C	c.1669G>A, p.G557R	1.12
P8	39/M	OD	ADRP [class B]	RHO	c.512C>G, p.P171R	_	-0.07
P9	40/F	OU	ADRP [class B]	RHO	c.50C>T, p.T17M	_	0.07
P10	19/M	OU	ARRP	PDE6B	c.1401+2T>G, p.?	c.175-246dup71, p.L83Cfs*19	0.10
P11	20/M	OU	ARRP	PDE6B	c.892C>T, p.Q298*	c.892C>T, p.Q298*	0.00
P12	61/M	OU	ARRP	PDE6B	c.2326G>A, p.D776N	c.2326G>A, p.D776N	0.05
P13	63/M	OD	ARRP	MAK	c.647T>C, p.L216S	c.647T>C, p.L216S	0.48
P14	23/M	OU	BCM	OPN1LW/MW	Exon 3 splice	_	0.90
P15	29/M	OU	BCM	OPN1LW/MW	c.607T>C, p.C203R	_	0.60
P16	16/F	OD	ESCS	NR2E3	c.119-2A>C, p.?	c.932G>A, p.R311Q	0.00
P17	20/M	OD	ESCS	NR2E3	c.119-2A>C, p.?	c.119-2A>C, p.?	0.04
P18	23/M	OD	ESCS	NR2E3	c.119-2A>C, p.?	c.932G>A, p.R311Q	0.42
P19	31/M	OD	ESCS	NR2E3	c.119-2A>C, p.?	c.932G>A, p.R311Q	0.80
P20	35/M	OD	ESCS	NR2E3	c.119-2A>C, p.?	c.767C>A, p.A256E	1.12

ADRP[Class B], autosomal dominant retinitis pigmentosa, Class B phenotype rod retained on perimetry; ARRP, autosomal recessive retinitis pigmentosa; BCM, blue cone monochromacy; BCVA, best-corrected visual acuity; cACHM, complete achromatopsia; ESCS, enhanced S-cone syndrome; iACHM[L/M], incomplete achromatopsia, L/M retained on perimetry; iACHM[S], incomplete achromatopsia, S retained on perimetry.

[†] Eye tested with perimetry, OD (right eye), OS (left eye), or OU (both eyes).

BCVA; average of two eyes when both eyes tested.

^{\$} Refused BCVA but previously recorded in the 0.3 to 0.5 logMAR range.

yellow background set at 100 cd·m⁻²; and 650BB, 650-nm stimuli on the 455-nm blue background set at 0.01 cd·m⁻². All stimuli were Goldmann size V equivalent 1.7° diameter and had a duration of 200 ms. All testing was performed with an 8-4-2 dB staircase algorithm. Sensitivity data are presented in dB units, which are the native units produced by the MonCvONE perimeter. In some cases, sensitivity data are converted to threshold by negation (e.g., +20 dB sensitivity is -20 dB threshold). All colors/conditions are calibrated such that 0 dB corresponds to 318 phot-cd·m⁻². Recordings were performed in healthy participants and patients with IRD along the vertical meridian extending to 30° eccentricity superior and inferior from fixation and sampled at 2° increments. Separate "foveal" sensitivities were obtained at fixation.

Fixation

A red steady light is used for testing nonfoveal locations in MonCvONE. There is also the choice of four red fixation lights used for testing foveal location. Both under darkadapted and light-adapted conditions, fixation luminance should ideally be "just visible" but not too bright. Normal eyes can see red fixation under all conditions proposed in the current work. However, IRD eyes with L/M-cone disease were unable to see either the single or the four red fixation lights at the brightest intensity under any of the three light-adapted conditions. In those cases, small black paper circles were attached at the location of the red fixation light(s) using nonpermanent clear adhesive tape.

Spectral Sensitivity Functions

Sensitivities recorded with four stimulus colors under dark-adapted conditions and on blue and yellow backgrounds of increasing intensity were first adjusted for energy and then fit with scotopic and photopic luminosity functions and with an S-cone spectral sensitivity function.¹³ Methods were similar to those previously described.^{7,15–17}

BACKGROUND ADAPTATION

Adaptation to different chromatic backgrounds was examined with the tvi paradigm. $^{18-23}$

Rod-mediated thresholds were fit using the following equation⁸:

$$y = 10 \left\{ log_{10} \left[\left(\frac{10^x + 10^{4_0}}{10^{4_0}} \right)^{n_0} \right] + log_{10} \left[\left(\frac{10^x + 10^{4_1}}{10^{4_1}} \right)^{n_1} \right] \right\}$$

where y is the threshold elevation above the dark-adapted value in dB units, x is the background luminance in \log_{10} units, A_0 is the low-luminance knee-point in \log_{10} units, n_0 is the slope of the low luminance section, A_1 is the saturation knee-point in \log_{10} units, and n_1 is the slope describing the saturation section.

Cone-mediated thresholds were fit using the following equation 17 :

$$y = 10 \left\{ log_{10} \left[\left(\frac{10^x + 10^{A_0}}{10^{A_0}} \right)^{n_0} \right] \right\}$$

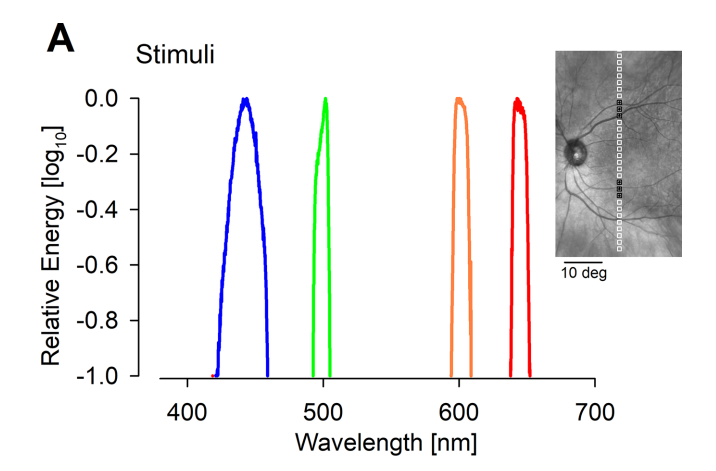
where y is the cone threshold elevation above the cone plateau (dark-adapted) value in dB units, x is the back-

ground luminance in \log_{10} units, A_0 is the low luminance knee-point in \log_{10} units, and n_0 is the slope of the low-luminance section. The best-fit model parameters were determined by minimizing the squared error (Solver, Excel, Microsoft 365) using the generalized reduced gradient method.

RESULTS

Determination of the Photoreceptor-Specific Test Conditions

The narrowband spectral distributions of the four chromatic stimuli in the short (440 and 500 nm) and long (600 and 650 nm) wavelength regimes are shown in Figure 1A. Two backgrounds built into the perimeter were used to evaluate sensitivity changes to chromatic stimuli as a function of chromatic light adaptation (Fig. 1B). One background appeared subjectively blue (455-nm peak) and the other appeared yellow (591-nm peak). The available dynamic ranges were -3.5 to +1.5 log cd·m⁻² for the blue background and -2.0 to +2.5 log cd·m⁻² for the yellow background; each could be adjusted in 0.5 log cd·m⁻² steps (Supplementary Table S1). Testing was also done under fully dark-adapted conditions. The measurements were performed at three neighboring retinal locations centered at 12° eccentricity in the supe-



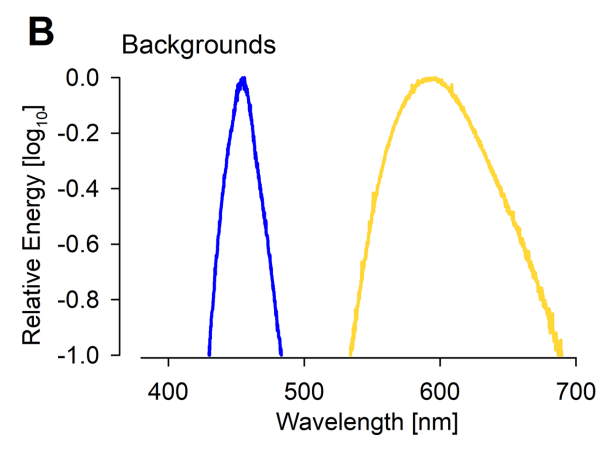


FIGURE 1. Relative spectral output of stimuli and backgrounds. (A) Normalized energy of the four narrowband stimuli (440, 500, 600, and 650 nm). *Inset*: Locations tested along the vertical meridian with profiles (*white squares*) and with the tvi paradigm (*dark squares*). (B) Normalized energy of the blue (455-nm peak) and yellow (591-nm peak) backgrounds.

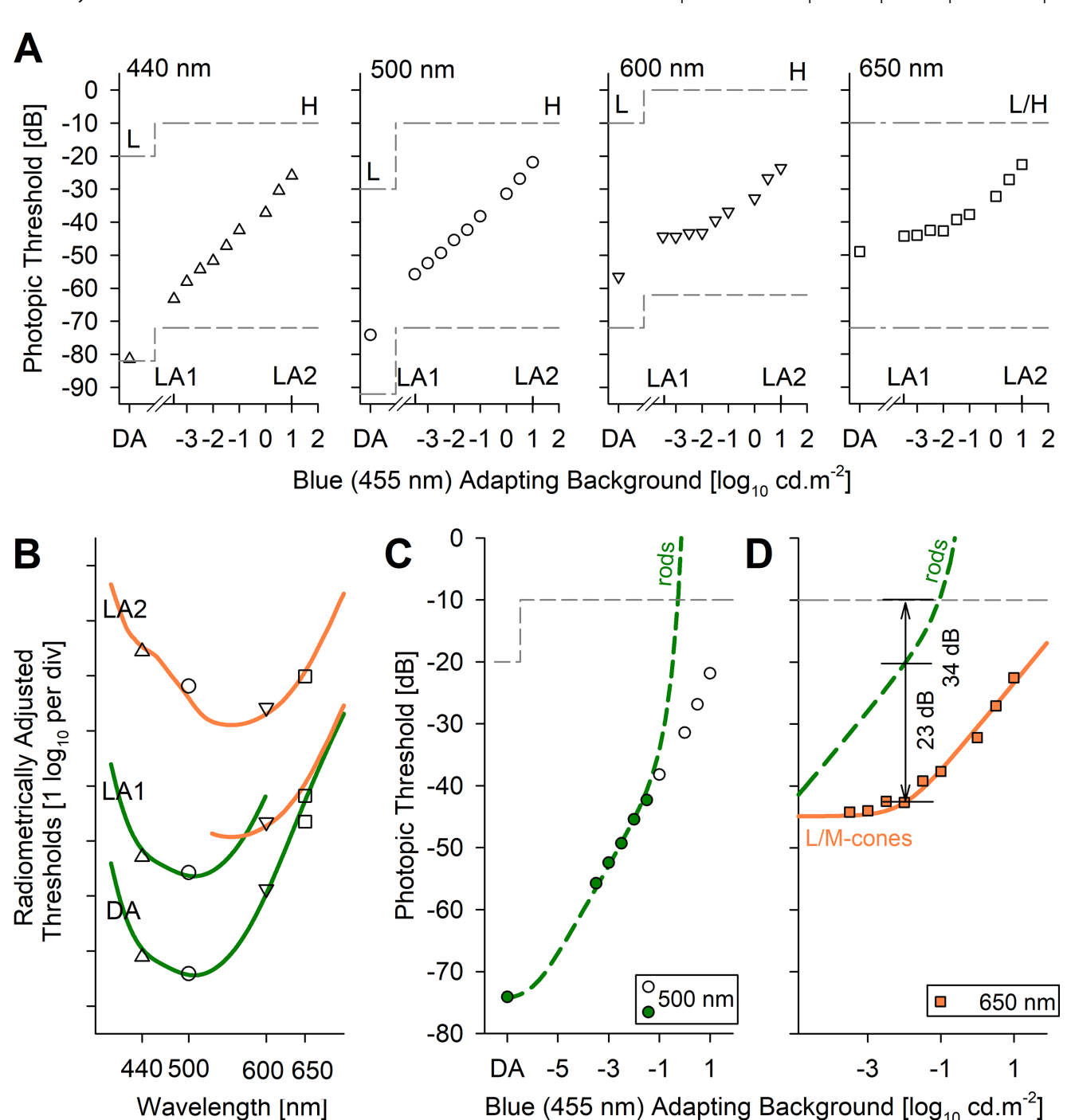


FIGURE 2. Adaptation and mediation of spectral sensitivities under dark-adapted conditions and with varying luminances of a blue background. (A) Thresholds for 440-, 500-, 600-, and 650-nm stimuli were evaluated under dark-adapted conditions and increasing amounts of blue background. Three notable conditions (DA, LA1, LA2) are evaluated further in panel B. Available technical dynamic ranges for low-luminance (L) and high-luminance (H) ranges are depicted with dashed lines. (B) Radiometrically adjusted thresholds under DA, -3.5 log cd·m⁻² (LA1), and +1.0 log cd·m⁻² (LA2) blue backgrounds plotted with luminosity functions for scotopic (green) and photopic (orange) vision. (C) The tvi curve (green) from thresholds for the 500-nm stimuli that fit the scotopic luminosity function (filled circles). (D) The tvi curve (green) vertically shifted. Effective physiological dynamic range and technical dynamic range are shown.

rior and inferior visual fields, selected to be near the rod hot spot²⁴ and avoid the macular pigment (Fig. 1A, inset).

To determine the optimal combination of stimulus and background that allows estimation of L/M-cone-specific function, we measured sensitivity to four stimuli under darkadapted (DA) conditions as well as on nine backgrounds with increasing blue light adaptation (LA) ranging from -3.5 to +1.0 log cd·m⁻² (Fig. 2A). The dimmest blue background elevated shorter-wavelength (440 and 500 nm) thresholds by 18 dB compared to DA. Long-wavelength (650 nm) thresholds, on the other hand, were only elevated by 3 dB compared to DA. Middle-wavelength (600 nm) thresholds

were intermediate with a 12-dB elevation. Over the next 1.5 log of background increases (between −3.5 and −2.0 log cd·m^{−2}), shorter wavelength thresholds continued incremental elevation. Long- and middle-wavelength thresholds showed no major changes and appeared to remain on a plateau. Across the higher range of backgrounds (between −1.5 and +1.0 log cd·m^{−2}), all four stimulus thresholds showed continuous elevations. Parsimony suggested that shorter wavelengths were likely driven by rods and Scones, whereas the longer wavelengths were driven by L/M-cones.

To confirm mediation across the conditions, CIE luminosity functions for scotopic and photopic vision were fit to DA thresholds and two notable blue background conditions, LA1 and LA2 (Fig. 2B). DA thresholds were well fit by the scotopic curve. Addition of the dimmest blue background (LA1) substantially changed the spectral sensitivity; shorter wavelengths continued to be mediated by scotopic vision (Fig. 2B, green curves), while thresholds to longer wavelengths were mediated by photopic vision (Fig. 2B, orange curves). Under the $+1.0 \log {\rm cd} \cdot {\rm m}^{-2}$ bright blue background (LA2), all four stimuli were mediated with photopic vision.

To better understand the potential involvement of rods in the long-wavelength regime, rod-mediated thresholds with the 500-nm stimulus were fit with the rod tvi model (Fig. 2C, green curve). The knee-point of the model occurred at -6.0log phot-cd·m⁻², and the apparent slope was 0.72. Next, the rod tvi model was transferred to 650 nm by vertically shifting to compensate for the DA threshold difference between 500 and 650 nm (Fig. 2D, green curve). Cone-mediated thresholds with the 650-nm stimulus were fit with the cone tvi model (Fig. 2D, orange curve). The blue background with $0.01 \text{ cd} \cdot \text{m}^{-2} \ (-2 \log_{10} \text{ cd} \cdot \text{m}^{-2})$ luminance was considered to represent a good compromise between the desire to obtain a cone-plateau estimate (which would require dimmer backgrounds) and the desire to retain a large physiological dynamic range before involvement of light-adapted rods (which would require brighter backgrounds). This condition, named 650BB (for a 650-nm stimulus on a blue background), appeared to be within 3 dB of the L/M-cone plateau threshold and retained more than a 20-dB physiological dynamic range before potential intrusion of normal rods. In patients with rod dysfunction, the dynamic range would likely be larger. Of note, the instrument dynamic range for this condition is 34 dB and should thus be able to accommodate testing of insensitive rods (Fig. 2D). Other retinal locations were not tested, but it is parsimonious to hypothesize that more centrally, L/M-cones would be more sensitive and rods less sensitive, and thus, the total physiological dynamic range would be larger.

To determine the optimal combination of stimulus and background that allows estimation of S-cone–specific function, we measured sensitivity to the same four chromatic stimuli DA, as well as on seven backgrounds with increasing amounts of yellow (591 nm) light, ranging from -1.0 to +2.0 log $cd\cdot m^{-2}$ (Fig. 3A). For 440-nm stimuli, the dimmest background elevated dark-adapted thresholds by 22 dB. From 0 to +1 log $cd\cdot m^{-2}$, 440-nm thresholds remained on an apparent plateau. Thereafter, there were incremental elevations with background. The other three stimuli showed continuous elevation with the background level throughout the range.

To confirm mediation across the stimuli and backgrounds, CIE luminosity functions for scotopic, photopic, and S-cone vision were fit to thresholds measured in the

dark-adapted state and on two notable yellow background conditions, LA1 and LA2 (Fig. 3B). Dark-adapted thresholds were well fit to the scotopic curve. Addition of the dimmest yellow background substantially changed the spectral sensitivity; shorter wavelengths (440 nm and 500 nm) continued to be mediated by scotopic vision (Fig. 3B, green curves) while thresholds to longer wavelengths were describable by photopic vision (Fig. 3B, orange curves). Under the +2.0 log cd·m⁻² bright yellow background, shorter-wavelength stimuli were mediated by S-cone vision (Fig. 3B, purple curve), whereas longer wavelengths remained driven by photopic vision.

The 500-nm stimuli mediated by scotopic vision were fit with the rod tvi model (Fig. 3C). The knee-point occurred at -3.07 log phot-log cd·m⁻², and the apparent slope was 1.02. Next, the rod tvi model was transferred to 440 nm by vertically shifting to compensate for the DA threshold difference between 500 and 440 nm (Fig. 3D, green curve). Cone-mediated thresholds with the 440-nm stimulus were fit with the cone tvi model (Fig. 3D, violet curve). The yellow background with 100 cd·m⁻² (2 log₁₀ cd·m⁻²) luminance was considered to represent a good balance between the desire to obtain a cone-plateau estimate (requiring dimmer backgrounds) and the desire to retain a large dynamic range before involvement of light-adapted rods (requiring brighter backgrounds). This condition, named 440YB (for 440 nm with a yellow background), appeared to be within 4 dB of the S-cone plateau threshold and retained more than a 17-dB physiological dynamic range before potential intrusion of normal rods. In patients with rod dysfunction, the dynamic range would likely be larger. Importantly, the instrument dynamic range for this condition is 35 dB (Fig. 3D).

Testing Protocol and Healthy Participants

Based on previous literature^{2,25} and results of the current work, five test conditions performed along the vertical meridian were chosen to form an informative test protocol that could be included in the workflow of an IRD clinic. The protocol consisted of pupillary dilation, 45 minutes of dark adaptation, followed by 650DA, 500DA, 650BB, and 440YB tests. Standard WhiteWB could be performed either before dark adaptation or between 650BB and 440YB tests. The latter approach saves testing time as the wait for dilation can be overlapped with the time for dark adaptation. For each test condition, first a vertical profile test was performed, followed by a fovea test. The total testing time was approximately 5 minutes per profile test and about 30 seconds per fovea test, adding up to 25 minutes per eye in addition to the dark adaptation period. All PERIRD consortium members provided data from at least two healthy participants. When data from both eyes of the same healthy participant were available, only the eye with the higher average sensitivity was included. Spurious sensitivity values that were more than 10 dB different from their immediate neighbors were censored (0.9% of 2356 thresholds obtained in controls and 0.4% of 4495 thresholds obtained in IRD eyes). Mean and 95% prediction intervals were calculated (Supplementary Fig. S1). Expected approximate cone-plateau thresholds (Supplementary Fig. S1, gray pluses) were overlaid on DA results, and approximate light-adapted rod sensitivities (Supplementary Fig. S1, gray squares) were overlaid on 650BB and 440YB results.

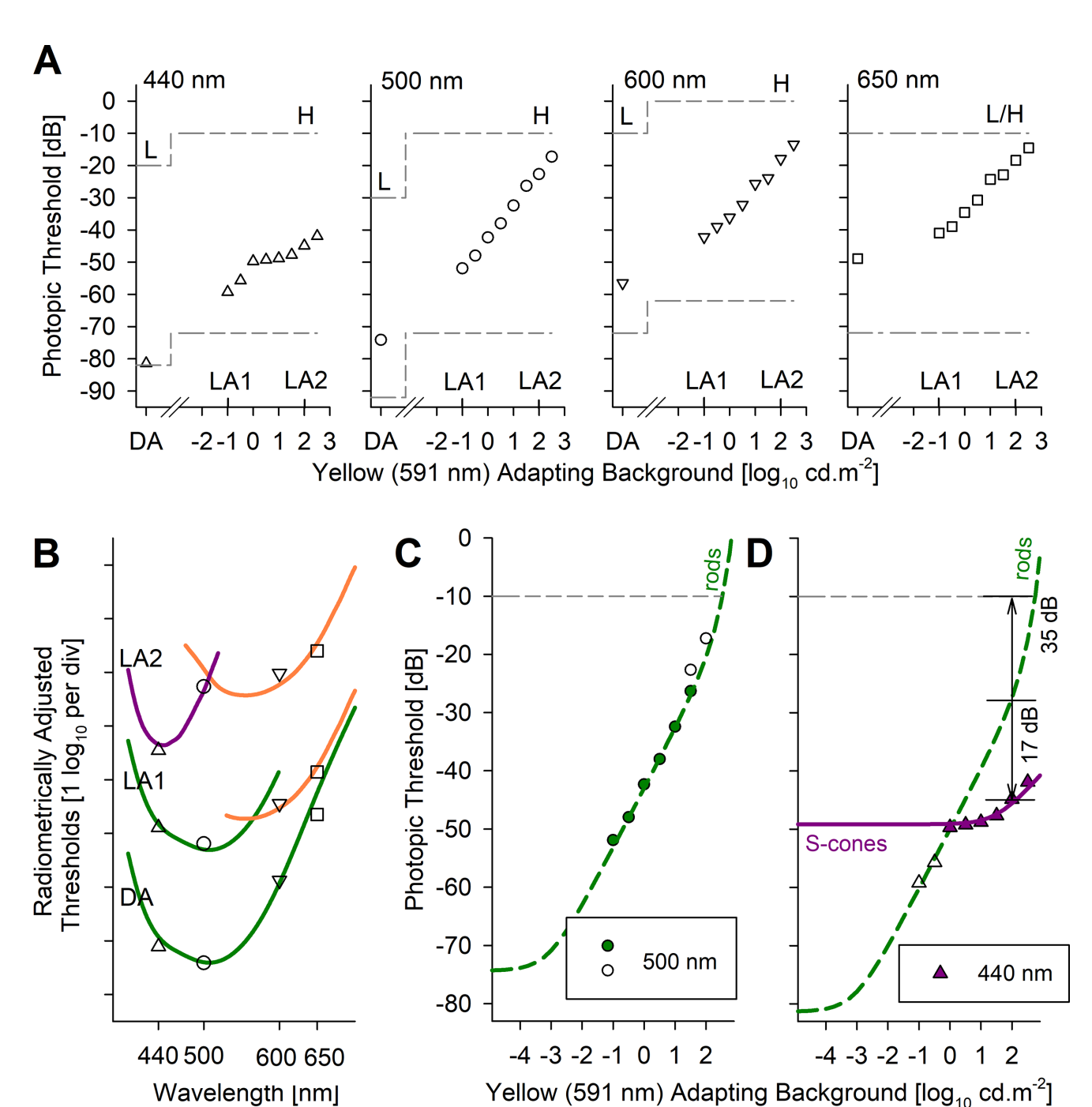


FIGURE 3. Adaptation and mediation of spectral sensitivities under dark-adapted conditions and with varying luminances of a yellow background. (A) Thresholds for 440-, 500-, 600-, and 650-nm stimuli were evaluated under dark-adapted conditions and increasing amounts of yellow background. Three notable conditions (DA, LA1, LA2) are evaluated further in panel B. Available technical dynamic ranges for low-luminance (L) and high-luminance (H) ranges are depicted with *dashed lines*. (B) Radiometrically adjusted thresholds under DA, -1.0 log cd·m⁻² (LA1), and +2.0 log cd·m⁻² (LA2) yellow backgrounds plotted with luminosity functions for scotopic (*green*), photopic (*orange*), and S-cone (*purple*) vision. (C) The tvi curve (*green*) from thresholds for 500-nm stimuli that fit the scotopic luminosity function (*filled triangles*) plotted together with the scotopic (*green*) tvi curve vertically shifted. Effective physiological dynamic range and technical dynamic range are shown.

Cone Dysfunction Syndromes and Related Retinal Diseases

An important consideration motivating the current work was to evaluate and distinguish between rod, L/M-cone, and S-cone function in IRDs and define both physiological

and technical limitations of photoreceptor identification in different circumstances. As a first test of the protocol, we evaluated molecularly clarified cone dysfunction syndromes and related conditions (Table), which included achromatopsia (ACHM),⁹ blue cone monochromacy (BCM),^{7,10} and enhanced S-cone syndrome (ESCS).^{26,27} In all three cases,

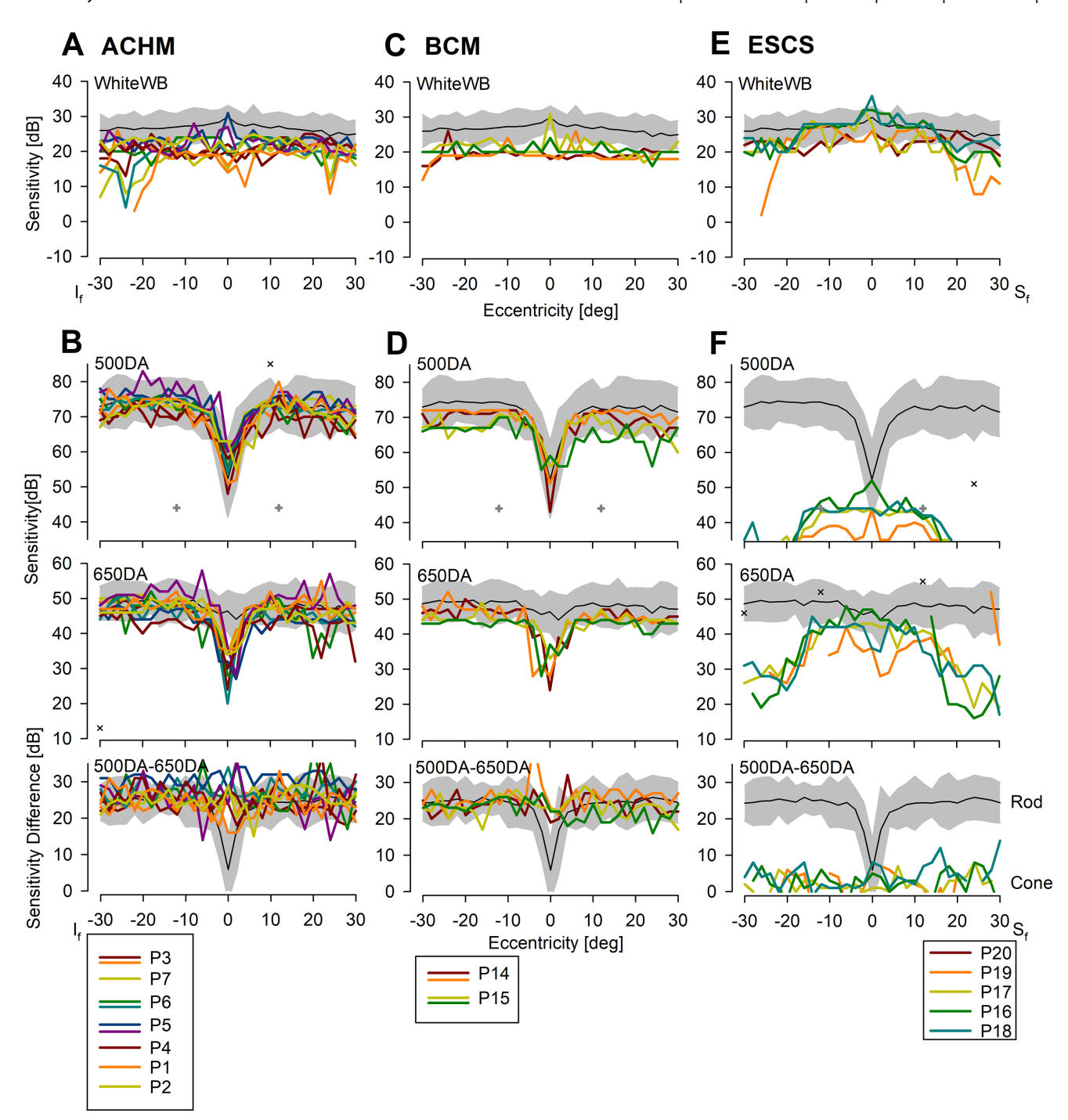


FIGURE 4. Standard and two-color dark-adapted perimetry results of three classic IRDs involving cones: ACHM, BCM, and ESCS. (A, C, E) Standard perimetry with white stimuli on a white background. (B, D, F) Two-color dark-adapted perimetry (*upper and middle panels*) and two-color differences (*lower panels*). Each colored trace represents an eye tested; some patients had both eyes tested and some only one eye. Censored data are marked with x. Cone-plateau sensitivities are shown with *gray pluses*. Normal ranges (*gray*) and mean normal values (*black*) are shown.

standard (WhiteWB) perimetry showed either normal or near-normal sensitivities (Figs. 4A, 4C, 4E), providing very little information to differentiate between these conditions, despite substantial differences in pathophysiology.

Two patients with CNGA3-ACHM (P2, P3) were clinically diagnosed with a complete form of ACHM (cACHM) with normal scotopic ERGs, undetectable photopic ERGs, lack of color vision, and poor visual acuity. Dark-adapted short-

wavelength (500DA) perimetric sensitivities were normal or near normal (Fig. 4B, upper panel), as expected. The only abnormality was the loss of dark-adapted long-wavelength (650DA) sensitivity near fixation (Fig. 4B, middle); mediation at this locus was suggestive of rods (Fig. 4B, lower). With cone-specific perimetry, both patients had reliably recordable 440YB and 650BB sensitivities, which were at the level of light-adapted rods (Fig. 5A, gray squares) or lower. Thus,

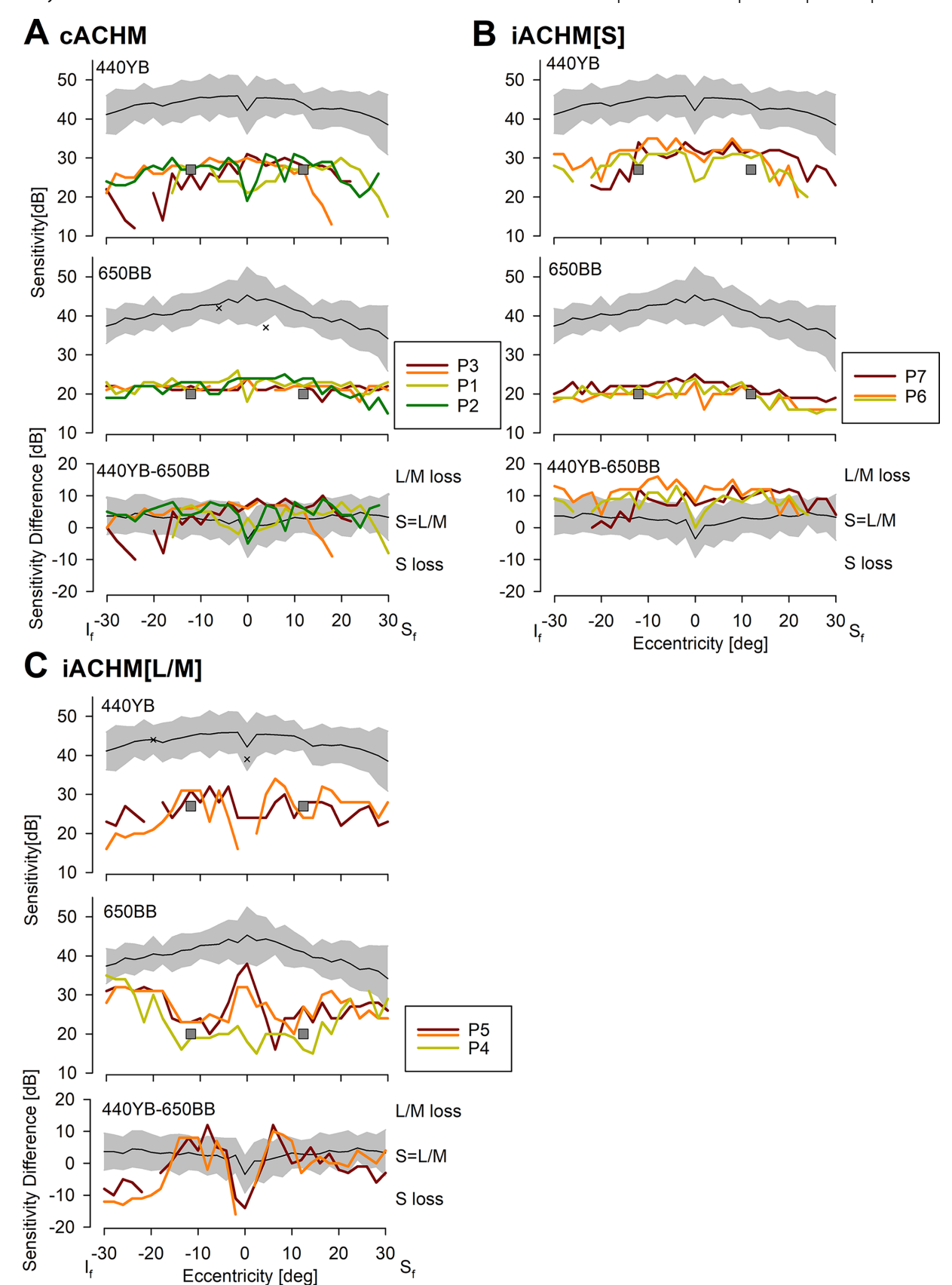


FIGURE 5. Cone-specific perimetry results in patients with ACHM with different phenotypes. (A) The cACHM phenotype corresponding to no detectable sensitivity with 440YB or 650BB beyond what could originate from light-adapted rods. (B) iACHM[S] showing macular evidence of S-cone function. (C) iACHM[L/M] centrally and peripherally. Note that P4 did not have 440YB results but is included here because the pattern of 650BB results is comparable to the two eyes of P5. Censored data are marked with x. Sensitivity expected from normal light-adapted rods is shown with *gray squares*.

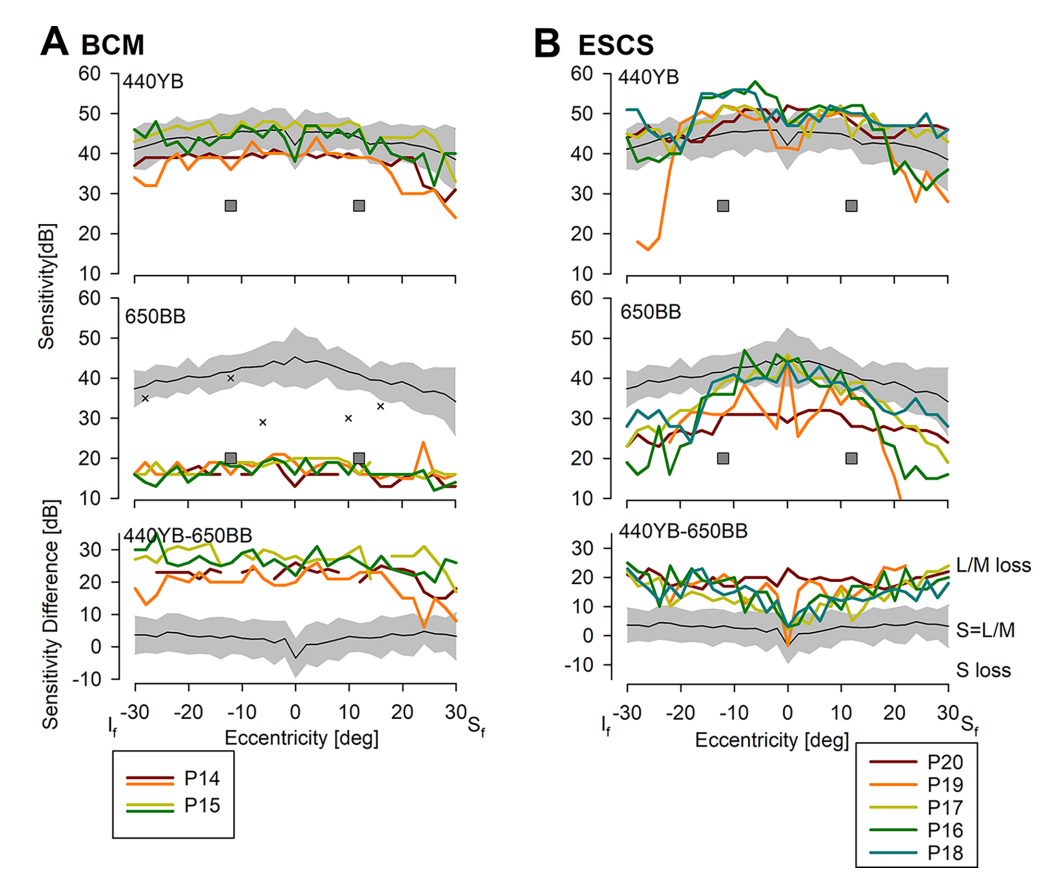


FIGURE 6. Cone-specific perimetry results in patients with BCM and ESCS. (A) Patients with BCM showing normal or near-normal 440YB results supporting S-cone function. With 650BB, results are consistent with mediation by light-adapted rods. (B) The patients with ESCS showing normal or hypernormal results on 440YB and normal or reduced results on 650BB. Censored data are marked with x. Sensitivity expected from normal light-adapted rods is shown with *gray squares*.

the perimetric phenotype of P2 and P3 was consistent with the clinical phenotype of cACHM. A patient with *CNGB3*-ACHM (P1) was also clinically diagnosed with cACHM; dark-adapted (Fig. 4B) and cone-specific (Fig. 5A) perimetric phenotypes were consistent with cACHM despite differences (*CNGA3* versus *CNGB3*) in molecular pathology.

Two additional patients with CNGA3-ACHM (P6, P7) are considered next. P7 had reduced acuities, abnormal color vision with no specific axis of confusion, retained scotopic ERG, undetectable flicker ERG, and a near-normal S-cone ERG. Molecularly, he had an intact red/green gene cluster but was compound heterozygous for two pathogenic CNGA3 variants. Clinical diagnosis was incomplete ACHM (iACHM). Dark-adapted perimetry was consistent with ACHM (Fig. 4B). Cone-specific perimetry showed 440YB results that were suggestive of detectable but reduced Scone sensitivities, which were up to 7 dB higher than the level expected from normal light-adapted rods (Fig. 5B, gray squares), whereas 650BB results could be explained by lightadapted rods (Fig. 5B, gray squares). Perimetric phenotype was iACHM with retained S-cones (iACHM[S]). P6 had limited clinical data, but based on her affected brother's results, she was considered to have cACHM. However, perimetric phenotype was consistent with iACHM[S] (Figs. 4B, 5B).

Another patient with *CNGA3*-ACHM (P5), who had a clinical diagnosis of iACHM with relatively retained acuities and a detectable cone ERG, had been extensively studied earlier. ²⁸ Dark-adapted perimetry was consistent with ACHM

(Fig. 4B). Cone-specific perimetry showed 440YB results that could be mostly explained by light-adapted rods (Fig. 5C, gray squares), whereas 650BB sensitivities were higher than the level for light-adapted rods (Fig. 5C, gray squares), and indeed approached the normal L/M-cone sensitivity range centrally and midperipherally (Fig. 5C). Perimetric phenotype was consistent with iACHM[L/M]. A similar 650BB perimetric phenotype of iACHM[L/M] was found in P4, who was clinically considered to have iACHM due to abnormal but substantially retained flicker ERG. Of note, P4 refused 440YB testing, stating that the yellow background adapting light was "too bright."

Two patients with BCM (P14, P15) showed dark-adapted perimetry similar to ACHM (Fig. 4D). With cone-specific testing, however, BCM results (Fig. 6A) were very different from all phenotypes of ACHM (Fig. 5). Specifically, patients with BCM had normal or near-normal S-cone sensitivity with 440YB (Fig. 6A, upper), whereas 650BB sensitivities were consistent with what would represent intrusion of normal light-adapted rod function and no L/M-cone function (Fig. 6A, middle, gray squares).

Another IRD with extreme effects on cone function is ESCS, ^{26,27} where 500DA sensitivities were reduced by more than 30 dB beyond the region near fixation (Fig. 4F, upper), consistent with congenital absence of all rods and all rod function. With 650DA, a macular mound of slightly reduced sensitivities was recorded, with a fall-off beyond 15° eccentricity (Fig. 4F, middle). Two-color sensitivity differences

between 500DA and 650DA were suggestive of pure cone function remaining (Fig. 4F, lower). With cone-specific testing, ESCS results showed 440YB sensitivities that were either within the normal range or hypernormal (Fig. 6B, upper). The 650BB sensitivities were within the normal range or reduced (Fig. 6B, middle). Considering there was no rod function in ESCS, all 440YB sensitivities can be assumed to be mediated by S-cones and all 650BB sensitivities mediated by L/M-cones. The 440YB minus 650BB differences across all patients were consistent with both absolute and relative hypersensitivity of the S-cones in this disease (Fig. 6B, lower)

Retinitis Pigmentosa and Related Retinal Diseases

Retinitis pigmentosa (RP), also known as rod-cone dystrophy, forms one of the most common diagnostic categories within IRDs. Photoreceptor-specific perimetry may contribute to the understanding of different phenotypes and disease stages of RP that generally affect rods earlier or to a greater extent than cones. We evaluated both autosomal recessive (AR) and autosomal dominant (AD) forms of RP.

Results from both eyes of two patients with PDE6Bassociated autosomal recessive retinitis pigmentosa (ARRP) (P10, P11) illustrate a commonly encountered stage of disease,5 where standard WhiteWB perimetry (Supplementary Fig. S2A) shows a central region of normal or nearnormal sensitivity that is surrounded by progressively greater losses with increasing eccentricity. Two-color darkadapted perimetry shows no evidence of rod function (Supplementary Figs. S2B-D). Centrally, with cone-specific testing, there are normal or near-normal sensitivities to Scones (Supplementary Fig. S2E) and L/M-cones (Supplementary Fig. S2F). Both types of cone-specific sensitivity profiles fall off with increasing eccentricity, but S-cone losses appear to lead L/M-cone losses (Supplementary Fig. S2G), potentially supporting a version of S-cone vulnerability described in RP²⁹ but localized to the leading edge of the photoreceptor degeneration wave.

Results from two older patients, one with *PDE6B*-ARRP (P12) and one with *MAK*-ARRP (P13), illustrate examples of more advanced disease. On standard perimetry, a smaller central area of retention is seen that is mediated by cones with no evidence of rods (Supplementary Figs. S3A–D). With cone-specific testing, S-cone sensitivities are reduced centrally and undetectable further eccentrically, but L/M-cone sensitivities are retained (Supplementary Figs. S3E–G). Superficially, this pattern of cone perimetry is suggestive of S-cone vulnerability, but it is important to note that both patients are older (Table). Spectral measurements²⁵ in cases like these could potentially differentiate between the effects of lens yellowing, S-cone vulnerability, or both.

Milder *RHO*-associated autosomal dominant retinitis pigmentosa (ADRP) class B³⁰ phenotypes (P8, P9) show retained central and midperipheral function on standard perimetry (Supplementary Fig. S4A). In P9, there is retained rod function that reaches near-normal levels by 30° eccentricity in the inferior field (Supplementary Figs. S4B–D). The apparent existence of perimacular reduced but rod-mediated function in this patient is likely an artifact of scattered light that occurs in eyes with large intraocular gradients, ranging from normal rod function to severe rod loss. Conespecific perimetry shows normal sensitivity to S- and L/M-cones centrally (Supplementary Figs. S4E, S4F), ruling out major effects from lens yellowing. With greater eccentric-

ity, however, S-cone losses are greater than L/M-cone losses (Supplementary Fig. S4G), potentially implicating a localized form of S-cone vulnerability.

Discussion

The primary molecular abnormalities in IRDs are often located in the photoreceptors, and thus predictably, the primary focus in the clinic is the resulting photoreceptor dysfunction. Since the basic function of photoreceptors is to signal light to higher visual centers, dysfunction of photoreceptors can be probed perceptually by measuring sensitivity to light. The spatial distribution of dysfunction, in turn, can be obtained with modern perimeters using computerized methods³ to stimulate focal regions across the retina and to keep track of the patients' responses. The PERIRD consortium was formed to develop clinically useful perimetric protocols that can be utilized to distinguish between rod, S-cone, and L/M-cone sensitivity at each retinal location and provide data toward deep phenotyping of genotyped IRDs that may be combined with imaging, electrophysiology, and other measures of visual function and retinal structure.

Spectral, temporal, spatial, and adaptation differences between photoreceptor types have been used in research settings to understand details of normal rod and cone vision, ^{18–22} consequences of glaucoma, ^{31–33} and distinguishing effects of IRDs on rods, ^{8,10,16,17,34} L/M-cones, and Scones.8,10,17 However, such studies tend to be performed on custom research equipment or modified equipment, or the protocols are too onerous to be usable routinely in the IRD clinic. The modified Humphrey visual field analyzer has been extensively used to perform photoreceptor-specific testing in the clinic. 4,5,9,30 The Octopus perimeter has been used with and without modification for two-color dark-adapted testing of rod and L/M-cone function.^{35–37} Unmodified Medmont DAC can perform two-color darkadapted testing clinically, but cone function measures are not possible on the same equipment.³⁸ Many clinical perimeters include short-wavelength automated perimetry³⁹⁻⁴¹ for S-cone specific measurements but do not include testing specific to rods or L/M-cones. Therefore, the current work considered designing a protocol with the unmodified MonCvONE perimeter^{25,42} to evaluate rod-, L/M-cone, and S-cone photoreceptor-specific function and evaluate visual function of a cohort of patients in IRD clinics across the international PERIRD consortium with duplicated instrumentation.

Four chromatic testing strategies were selected to provide photoreceptor-specific sensitivity estimates. Beyond $\sim 5^{\circ}$ of eccentricity, 500DA/650DA testing evaluated rod function, 440YB testing evaluated S-cone function, and 650BB testing evaluated L/M-cone function. The instrument (technical) dynamic ranges were at least 62 dB and could be as large as 82 dB, depending on the stimulus. The physiological dynamic ranges could be reduced due to the involvement of multiple photoreceptor populations. For example, the physiological range of the 500DA stimulus for measuring rods was about 30 dB before normal dark-adapted cones may intrude (thus, up to 30 dB of rod sensitivity loss is measurable in patients with normal cone sensitivity). The physiological range of the 440YB stimulus for measuring S-cones was about 20 dB before normal light-adapted rod function may intrude (thus, up to 20 dB of S-cone sensitivity loss is measurable in patients with normal rod sensitivity). However, in most IRDs, potentially intruding photoreceptors are often not normal, and thus, physiological dynamic ranges could be larger than in these worst-case scenarios. Future studies that consider such factors would need to perform spectral sensitivity functions²⁵ at one or more locations to definitively identify photoreceptor sources.

The central macular region between the fovea and 5° eccentricity requires special consideration. First, the interindividual variation of macular pigment density^{43–45} tends to absorb shorter-wavelength stimuli, such as the 440YB and 500DA, but does not appreciably absorb longerwavelength stimuli, such as 650BB and 650DA, used in the current work. Second, as the foveal area is approached, there is a reduction of rod cell density, shortening of rod outer segments, and an increase of cone cell density and cone outer segment lengths.7,24 The major drop in normal sensitivity with 500DA in this central region is likely driven by a complex combination of underlying macular pigment and rod changes. The lack of major change with 650DA in the central macula in normal eyes, on the other hand, is likely driven by the smooth conversion from rod mediation eccentrically to L/M-cone mediation centrally, as apparent from the difference (500DA-650DA) plots. Unlike 650DA, the 650BB is L/M-cone mediated throughout, and the profile shows a peak centrally dropping off eccentrically, as expected from the relatively shallow photopic hill of a large stimulus.

In cone dysfunction syndromes affecting foveal L/M-cones, visual acuity is reduced, and fixation is often near the fovea 10 but not stable. As long as fixation is within the central macula, it is highly likely that eccentric results produced by the perimetry are generally interpretable and repeatable, except for the immediate region near fixation. However, in cases of large central atrophy or eccentric fixation beyond $\pm 3^{\circ}$ from anatomic fovea, interpretation of standard perimeter results becomes more tenuous, and retina-tracking techniques such as microperimetry may be considered.

For some forms or stages of IRD, an S-cone vulnerability has been previously described, where S-cone function is relatively more affected compared to L/M-cone function in terms of acuity, ERG, psychophysics, color vision, or adaptive optics (AO)-OCT. 29,46-50 Here we propose to calculate the difference between 440YB and 650BB sensitivities to estimate the spatial distribution of any imbalance that may exist between L/M- and S-cone function across the functional retina. Our illustrative examples showed imbalances favoring S-cones in ESCS and BCM, or favoring S- or L/M-cones in iACHM. In rod-cone dystrophies, surprisingly, there could be central regions of normal S- and L/M-cones surrounded by apparent vulnerability of S-cones. In cases where S-cone function is reduced throughout the visual field, it is important to consider a potential artifact in participants older than 50 years, as the human lens tends to increasingly yellow with age.51 Short-wavelength stimuli are preferentially absorbed by the yellow lens, giving the impression of an apparent Scone vulnerability throughout the remaining visual field. If necessary, the extent of lens yellowing can be estimated with perceptual or imaging approaches.⁵²

All perimetric instruments perform some sampling of the visual field in terms of extent, pattern, and spatial distribution. For the current work, we strived to have several perimetric tests that are each less than 5 minutes in duration and extended to the midperiphery. Based on previous experience, we settled on a unidimensional profile test extending vertically to 30° eccentricity with 2° sampling density. Among the alternatives would be performing the measures

along the horizontal meridian. Although a horizontal sensitivity profile provides indirect evidence of central fixation by revealing the expected position of the blind spot in relationship to fixation, the test also carries a limitation, as approximately 15% to 20% of the sensitivity samples obtained near the blind spot may be uninterpretable. The symmetry around fixation of the vertical sensitivity profile and of the underlying retinal structure allows for hemifield comparisons. This is particularly useful in IRDs, as several molecular forms often show a predilection for earlier abnormalities in the superior and/or inferior perifovea or near midperiphery, which can be monitored by the vertical profile. In addition, subretinal gene therapy trials usually treat the superior retina near the vertical meridian, which would allow comparisons between treated and control untreated retinas on vertical sensitivity profiles. However, in certain IRDs or with certain treatments, different patterns and extents may have to be used to answer specific questions regarding phenotype, natural history, or outcome of interventions.

To illustrate the interpretation of the results of our proposed protocol, we evaluated IRDs with ESCS and classic cone dysfunction syndromes BCM and ACHM. ESCS allowed understanding of photoreceptor-specific visual function in retinas devoid of rods, with only S- and L/M-cones remaining. BCM, on the other hand, illustrated retinas with normal rod function and normal S-cones but lacking L/M-cone function. ACHM involves retina-wide cone dysfunction but tends to present a greater spectrum of phenotypic complexity compared to BCM and ESCS,53 and our preliminary results with photoreceptor-specific perimetry further expand upon that complexity. ACHM is clinically subcategorized into complete and incomplete forms mainly based on full-field ERG results. Generally, complete ACHM shows no ERG evidence of functioning cones, whereas incomplete ACHM shows abnormal but recordable cone ERGs. There have been only limited studies of incomplete ACHM using perceptual measures,²⁸ and we are not aware of any perceptual studies that attempted to map the remnant cone function across the visual field, as done in the current work. In this preliminary study, there appeared to be a differentiation between patients with ACHM retaining remnant S-cone function but not L/M-cone function, which we named the iACHM[S] phenotype, or remnant L/M-cone function but not S-cone function, named iACHM[L/M]. Some of these patients had recordable cone ERGs, as expected from incomplete ACHM, but others did not. Assuming the existence of these perimetric phenotypes is confirmed with further studies, our findings appear to imply that patients with not only incomplete ACHM but also a subset of clinically complete ACHM may retain perimetrically detectable cone function. This finding would be not unlike the phenotype of oligocone trichromacy, which molecularly overlaps with ACHM and demonstrates retained central cone function despite undetectable or severely reduced cone ERGs.54,55

In addition to phenotyping and natural history studies, our proposed photoreceptor-specific perimetry protocol could contribute to informative outcome measures for clinical trials attempting to arrest progression or improve vision in IRDs. Outcomes used to date in early- and latephase trials have included unmodified commercial devices performing standard perimetry⁵⁶ and mesopic microperimetry,⁵⁷ both of which cannot distinguish between rods and cones. Chromatic dark-adapted and light-adapted perimetry using modified instruments can distinguish between rods and L/M-cones.^{58,59} We are not aware of any perimetric eval-

uation of S-cone function in IRD clinical trials, despite the widespread availability of this method in many commercial devices. The protocol described herein promises to provide rod, L/M-cone, and S-cone–specific measures of visual function over a large dynamic range using a commercially available perimeter and a relatively short, practical protocol that may be introduced in the clinic, translational work, and clinical trials. ^{25,60–62}

Acknowledgments

Supported by Blue Cone Monochromacy Families Foundation, Italian Achromatopsia Association, Samuel G. Jacobson, MD, PhD, Memorial Fund, and Research to Prevent Blindness.

Disclosure: V. Wu, None; A.J. Roman, None; E.L. Galsterer, None; G. Ansari, None; I. Erdinest, None; G. Righetti, None; I. Viarbitskaya, None; R.C. Russell, None; R.J. Kim, None; J. Charlier, Metrovision (E); K. Pfau, None; K. Stingl, None; E. Banin, None; M. Pfau, None; K. Stingl, None; T.S. Aleman, None; A.V. Cideciyan, None

References

- Hood DC, Finkelstein MA. Sensitivity to light. In: Boff K, Kaufman L, Thomas J, eds. *Handbook of Perception and Performance*. New York, NY: Wiley; 1986:5–66.
- Cideciyan AV, Krishnan AK, Roman AJ, Sumaroka A, Swider M, Jacobson SG. Measures of function and structure to determine phenotypic features, natural history, and treatment outcomes in inherited retinal diseases. *Annu Rev Vis Sci*. 2021;7(1):747–772.
- 3. Johnson CA. Psychophysical factors that have been applied to clinical perimetry. *Vis Res.* 2013;90:25–31.
- Jacobson SG, Voigt WJ, Parel JM, et al. Automated light- and dark-adapted perimetry for evaluating retinitis pigmentosa. *Ophthalmology*. 1986;93(12):1604–1611.
- Jacobson SG, Roman AJ, Aleman TS, et al. Normal central retinal function and structure preserved in retinitis pigmentosa. *Invest Ophthalmol Vis Sci.* 2010;51(2):1079–1085.
- Milam AH, Rose L, Cideciyan AV, et al. The nuclear receptor NR2E3 plays a role in human retinal photoreceptor differentiation and degeneration. *Proc Natl Acad Sci USA*. 2002;99(1):473–478.
- Cideciyan AV, Hufnagel RB, Carroll J, et al. Human cone visual pigment deletions spare sufficient photoreceptors to warrant gene therapy. *Hum Gene Ther*. 2013;24(12):993– 1006
- Jacobson SG, Cideciyan AV, Peshenko IV, et al. Determining consequences of retinal membrane guanylyl cyclase (RetGC1) deficiency in human Leber congenital amaurosis en route to therapy: residual cone-photoreceptor vision correlates with biochemical properties of the mutants. *Hum Mol Genet*. 2013;22(1):168–183.
- Zelinger L, Cideciyan AV, Kohl S, et al. Genetics and disease expression in the CNGA3 form of achromatopsia: steps on the path to gene therapy. *Ophthalmology*. 2015;122(5):997– 1007.
- Luo X, Cideciyan AV, Iannaccone A, et al. Blue cone monochromacy: visual function and efficacy outcome measures for clinical trials. PLoS ONE. 2015;10(4):e0125700.
- Tikidji-Hamburyan A, Reinhard K, Storchi R, et al. Rods progressively escape saturation to drive visual responses in daylight conditions. *Nat Communs*. 2017;8(1):1813.
- 12. Frederiksen R, Morshedian A, Tripathy SA, et al. Rod photoreceptors avoid saturation in bright light by the movement of the G protein transducin. *J Neurosci*. 2021;41(15):3320–3330.

- Stockman A, Sharpe LT, Fach C. The spectral sensitivity of the human short-wavelength sensitive cones derived from thresholds and color matches. Vis Res. 1999;39(17):2901– 2927
- Stockman A, Sharpe LT. The spectral sensitivities of the middle- and long-wavelength-sensitive cones derived from measurements in observers of known genotype. *Vis Res*. 2000;40(13):1711–1737.
- 15. Cideciyan AV, Pugh EN, Lamb TD, Huang Y, Jacobson SG. Rod plateaux during dark adaptation in Sorsby's fundus dystrophy and vitamin A deficiency. *Invest Ophthalmol Vis Sci.* 1997;38(9):1786–1794.
- Cideciyan AV, Zhao X, Nielsen L, Khani SC, Jacobson SG, Palczewski K. Null mutation in the rhodopsin kinase gene slows recovery kinetics of rod and cone phototransduction in man. *Proc Natl Acad Sci USA*. 1998;95(1):328–333.
- 17. Cideciyan AV, Haeseleer F, Fariss RN, et al. Rod and cone visual cycle consequences of a null mutation in the 11-cis-retinol dehydrogenase gene in man. *Vis Neurosci*. 2000;17(5):667–678.
- Aguilar M, Stiles WS. Saturation of the rod mechanism of the retina at high levels of stimulation. *Optica Acta*. 1954;1:59– 65.
- 19. Fuortes MG, Gunkel RD, Rushton WA. Increment thresholds in a subject deficient in cone vision. *J Physiol*. 1961;156(1):179–192.
- Blakemore CB, Rushton WA. Dark adaptation and increment threshold in a rod monochromat. *J Physiol*. 1965;181(3):612– 628.
- 21. Blakemore CB, Rushton WA. The rod increment threshold during dark adaptation in normal and rod monochromat. *J Physiol.* 1965;181(3):629–640.
- 22. Sharpe LT, Fach C, Nordby K, Stockman A. The incremental threshold of the rod visual system and Weber's law. *Science*. 1989;244(4902):354–356.
- 23. Simunovic MP, Hess K, Avery N, Mammo Z. Threshold versus intensity functions in two-colour automated perimetry. *Ophthalmic Physiol Opt.* 2021;41:157–164.
- 24. Curcio CA, Sloan KR, Kalina RE, Hendrickson AE. Human photoreceptor topography. *J Comp Neurol*. 1990;292(4):497–523.
- 25. Cideciyan AV, Roman AJ, Warner RL, et al. Evaluation of retinal structure and visual function in blue cone monochromacy to develop clinical endpoints for L-opsin gene therapy. *Int J Mol Sci.* 2024;25(19):10639.
- 26. Garafalo AV, Calzetti G, Cideciyan AV, et al. Cone vision changes in the enhanced S-cone syndrome caused by NR2E3 gene mutations. *Invest Ophthalmol Vis Sci.* 2018;59(8):3209–3219.
- 27. Roman AJ, Powers CA, Semenov EP, et al. Short-wavelength sensitive cone (S-cone) testing as an outcome measure for NR2E3 clinical treatment trials. *Int J Mol Sci.* 2019;20(10):2497–2497.
- 28. Trankner D, Jagle H, Kohl S, et al. Molecular basis of an inherited form of incomplete achromatopsia. *J Neurosci*. 2004;24(1):138–147.
- Swanson WH, Birch DG, Anderson JL. S-cone function in patients with retinitis pigmentosa. *Invest Ophthalmol Vis Sci.* 1993;34(11):3045–3055.
- Cideciyan AV, Hood DC, Huang Y, et al. Disease sequence from mutant rhodopsin allele to rod and cone photoreceptor degeneration in man. *Proc Natl Acad Sci USA*. 1998;95(12):7103–7108.
- 31. Harwerth RS, Smith EL, III, DeSantis L. Mechanisms mediating visual detection in static perimetry. *Invest Ophthalmol Vis Sci.* 1993;34(10):3011–3023.
- 32. Harwerth RS, Carter-Dawson L, Shen F, Smith EL, III, Crawford ML. Ganglion cell losses underlying visual field defects

- from experimental glaucoma. *Invest Ophthalmol Vis Sci.* 1999;40(10):2242–2250.
- 33. Harwerth RS, Smith EL, III, Chandler M. Progressive visual field defects from experimental glaucoma: measurements with white and colored stimuli. *Optom Vis Sci.* 1999;76(8):558–570.
- 34. Hood DC, Greenstein V. Models of the normal and abnormal rod system. *Vis Res.* 1990;30(1):51–68.
- Birch DG, Herman WK, deFaller JM, Disbrow DT, Birch EE. The relationship between rod perimetric thresholds and full-field rod ERGs in retinitis pigmentosa. *Invest Ophthal*mol Vis Sci. 1987;28(6):954–965.
- Igelman AD, Park JC, Hyde RA, et al. Two-color darkadapted perimetry implemented with a commercially available perimeter to characterize rod-pathway sensitivity. Ophthalmic Surg Lasers Imaging Retina. 2022;53(12):692– 696.
- 37. Ku CA, Igelman AD, Huang SJ, et al. Improved rod sensitivity as assessed by two-color dark-adapted perimetry in patients with RPE65-related retinopathy treated with voretigene neparvovec-rzyl. *Transl Vis Sci Technol*. 2023;12 (4):17.
- 38. Bennett LD, Klein M, Locke KG, Kiser K, Birch DG. Dark-adapted chromatic perimetry for measuring rod visual fields in patients with retinitis pigmentosa. *Transl Vis Sci Technol*. 2017;6(4):15.
- 39. Sample PA, Taylor JD, Martinez GA, Lusky M, Weinreb RN. Short-wavelength color visual fields in glaucoma suspects at risk. *Am J Ophthalmol*. 1993;115(2):225–233.
- Sample PA, Johnson CA, Haegerstrom-Portnoy G, Adams AJ. Optimum parameters for short-wavelength automated perimetry. *J Glaucoma*. 1996;5(6):375–383.
- 41. Demirel S, Johnson CA. Isolation of short-wavelength sensitive mechanisms in normal and glaucomatous visual field regions. *J Glaucoma*. 2000;9(1):63–73.
- 42. Li RTH, Roman AJ, Sumaroka A, et al. Treatment strategy with gene editing for late-onset retinal degeneration caused by a founder variant in C1QTNF5. *Invest Ophthalmol Vis Sci.* 2023;64(15):33.
- 43. Snodderly DM, Brown PK, Delori FC, Auran JD. The macular pigment. I. Absorbance spectra, localization, and discrimination from other yellow pigments in primate retinas. *Invest Ophthalmol Vis Sci.* 1984;25(6):660–673.
- Snodderly DM, Auran JD, Delori FC. The macular pigment.
 II. Spatial distribution in primate retinas. *Invest Ophthalmol Vis Sci.* 1984;25(6):674–685.
- Aleman TS, Duncan JL, Bieber ML, et al. Macular pigment and lutein supplementation in retinitis pigmentosa and Usher syndrome. *Invest Ophthalmol Vis Sci.* 2001;42(8):1873–1881.
- 46. Greenstein VC, Hood DC, Ritch R, Steinberger D, Carr RE. S (blue) cone pathway vulnerability in retinitis pigmentosa, diabetes and glaucoma. *Invest Ophthalmol Vis Sci.* 1989;30(8):1732–1737.

- 47. Yamamoto S, Hayashi M, Tsuruoka M, et al. Selective reduction of S-cone response and on-response in the cone electroretinograms of patients with X-linked retinoschisis. *Graefes Arch Clin Exp Ophthalmol*. 2002;240(6):457–460.
- 48. Vincent A, Robson AG, Neveu MM, et al. A phenotypegenotype correlation study of X-linked retinoschisis. *Ophthalmology*. 2013;120(7):1454–1464.
- Jolly JK, Simunovic MP, Dubis AM, et al. Structural and functional characteristics of color vision changes in choroideremia. Front Neurosci. 2021;15:729807.
- 50. Lassoued A, Zhang F, Kurokawa K, et al. Cone photoreceptor dysfunction in retinitis pigmentosa revealed by optoretinography. *Proc Natl Acad Sci USA*. 2021;118(47):e2107444118.
- 51. Johnson CA, Marshall D, Jr. Aging effects for opponent mechanisms in the central visual field. *Optom Vis Sci.* 1995;72(2):75–82.
- 52. Charng J, Tan R, Luu CD, et al. Imaging lenticular autofluorescence in older subjects. *Invest Ophtbalmol Vis Sci.* 2017;58(12):4940–4947.
- Aboshiha J, Dubis AM, Carroll J, Hardcastle AJ, Michaelides M. The cone dysfunction syndromes. Br J Ophthalmol. 2016;100(1):115–121.
- 54. Michaelides M, Holder GE, Bradshaw K, Hunt DM, Mollon JD, Moore AT. Oligocone trichromacy: a rare and unusual cone dysfunction syndrome. *Br J Ophthalmol*. 2004;88(4):497–500.
- 55. Andersen MK, Christoffersen NL, Sander B, et al. Oligocone trichromacy: clinical and molecular genetic investigations. *Invest Ophthalmol Vis Sci.* 2010;51(1):89–95.
- 56. Russell S, Bennett J, Wellman JA, et al. Efficacy and safety of voretigene neparvovec (AAV2-hRPE65v2) in patients with RPE65-mediated inherited retinal dystrophy: a randomised, controlled, open-label, phase 3 trial. *Lancet*. 2017;390(10097):849–860.
- 57. Igoe JM, Lam BL, Gregori NZ. Update on clinical trial endpoints in gene therapy trials for inherited retinal diseases. *J Clin Med.* 2024;13(18):5512.
- 58. Jacobson SG, Cideciyan AV, Ratnakaram R, et al. Gene therapy for Leber congenital amaurosis caused by RPE65 mutations: safety and efficacy in 15 children and adults followed up to 3 years. *Arch Ophthalmol*. 2012;130(1):9–24.
- 59. Jacobson SG, Cideciyan AV, Ho AC, et al. Night vision restored in days after decades of congenital blindness. *iScience*. 2022;25(10):105274.
- Farahbakhsh M, Anderson EJ, RO, et al. A demonstration of cone function plasticity after gene therapy in achromatopsia. *Brain*. 2022;145(11):3803–3815.
- McKyton A, Marks Ohana D, Nahmany E, Banin E, Levin N. Seeing color following gene augmentation therapy in achromatopsia. *Curr Biol.* 2023;33(16):3489–3494.
- 62. Anderson EJ, Dekker TM, Farahbakhsh M, et al. fMRI and gene therapy in adults with CNGB3 mutation. *Brain Res Bull*. 2024;215:111026.